PERGAMON

International Journal of Heat and Mass Transfer 45 (2002) 4925–4936

International Journal of HEAT and MASS TRANSFER

www.elsevier.com/locate/ijhmt

Heat exchange in an attic space

P.M. Haese *, M.D. Teubner

Department of Applied Mathematics, University of Adelaide, Adelaide, Australia 5005

Received 18 May 2001; received in revised form 31 May 2002

Abstract

Thermal effects in building attics are extremely important in regions where temperature extremes occur regularly. In particular, in the northern regions of North America, cold winters can lead to a dangerous build-up of ice on roofs, as well as preventing heat being distributed efficiently through the building. This paper examines heat transfer within attics and looks at an inexpensive solution technique involving ceiling fans. The computer model developed accurately reproduces the results of previous investigations, presents solutions for realistic Grashof numbers, and demonstrates the effects of installing ceiling fans in the ceilings of top storey rooms in affected buildings.

1. Introduction

The Copper Chase Condominiums are part of the Brian Head Ski Resort in Utah, USA. Situated some 214 miles from Las Vegas, Nevada, Brian Head is a picturesque region reknown for snow sports in the winter and a variety of other outdoor attractions in summer, including Bryce Canyon and Zion National Parks, and Cedar Breaks National Monument.

One of the two condominium buildings, the Lodge building, is east-west oriented, about 50 m × 22 m and is three storeys high. It has a central atrium which goes from the ground floor right to the top of the building. There is a section attached to the south side of the building which houses a swimming pool and jacuzzi, and another enclosed area on the north side of the building.

The Lodge building has two temperature-related problems. Firstly, because the building is east-west oriented and lies at latitude 37.5° N, the north side of the roof sees no sun in winter. Consequently, snow collects on this side of the roof and compacts to ice. There is a serious danger of the roof collapsing under the weight, and further, when the spring warmth begins to melt the ice, it slides off, which is extremely dangerous for any people below. The ice has also been known to go through the roof of the section attached to the north side of the building. Secondly, due to the central atrium and the fact that only the ground floor is air conditioned, rooms on the top floor get too hot in both summer and winter.

Whilst there are many methods for melting ice on roofs currently in use, all have disadvantages. Roof sprinklers are not able to be used because the water would freeze in the pipes. Also popular are heating cables; however, requiring some 50 W per square meter, these are not economically feasible for such a big roof.

In this paper, we explore the possibility of putting vents in the ceiling of the third floor to allow hot air to rise into and circulate through the attic. Our aim is to heat the attic sufficiently in winter to melt the ice through the roofing material, thus preventing its collection on the roof. In summer, such vents would allow excess heat from the third floor to move into the attic space.

Heat exchange in an attic space is not a new area of research, having already been investigated by a number of researchers, including Akinsete and Coleman [1], Poulikakos and Bejan [2], del Campo et al. [3] and recently by Hasani and Chung [4]. All these investigations have had a fundamental problem, however, namely the magnitude of the Rayleigh number they used for their flows. In the study by Akinsete and Coleman [1], for example, the maximum value for Ra used was 4.5×10^4.

* Corresponding author.

E-mail address: phaese@maths.adelaide.edu.au (P.M. Haese).

0017-9310/02/$ - see front matter
PII: S0017-9310(02)00208-9

Nomenclature

c_p	specific heat at constant pressure, $J\,kg^{-1}\,K^{-1}$
g	acceleration due to gravity, $N\,m^{-3}$
Gr	Grashof number
H	height of the enclosure, m
P	pressure, Pa
Pr	Prandtl number
q	velocity vector, $m\,s^{-1}$
Ra	Rayleigh number
t	non-dimensional time
T	absolute temperature, K
u, v	x,y-components of velocity, $m\,s^{-1}$
v_{in}	non-dimensional inflow velocity
U, V	x,y-components of non-dimensional velocity
x, y	Cartesian coordinates in horizontal and vertical directions, respectively, m
X, Y	non-dimensional x,y-coordinates
α	thermal diffusivity, $m^2\,s^{-1}$
β	coefficient of thermal expansion, K^{-1}
Δx, Δy	grid spacings in the x and y-directions, respectively
θ	non-dimensional temperature
λ	thermal conductivity, $J\,K^{-1}\,m^{-1}\,s^{-1}$
μ	dynamic viscosity, $kg\,m^{-1}\,s^{-1}$
ν	kinematic viscosity, $m^2\,s^{-1}$
ρ	fluid density, $kg\,m^{-3}$
Ψ	non-dimensional stream function
Ω	non-dimensional vorticity

Hasani and Chung [4] stated that this range was too small, claiming that "in reality, values of Ra as high as 10^6 can be encountered in such enclosures". However, for a realistic attic we expect the Rayleigh number to be of order 10^{10} or 10^{11}.

In this article, we set out to examine the possibility of modelling attic flow with realistic Rayleigh numbers.

2. Problem formulation

Following Akinsete and Coleman [1], we consider the two-dimensional flow of an ideal fluid. We neglect both viscous dissipation and compressibility effects and assume fluid properties to be constant except in the body force term in accordance with the Boussinesq approximation. Under these conditions, we may write down the following set of dimensionless equations (1)–(5) governing the flow, as described by Hasani and Chung [4]:

Vorticity transport equation:

$$\frac{\partial \Omega}{\partial t} + \vec{q} \cdot \vec{\nabla}\Omega = \nabla^2 \Omega + \frac{Ra}{Pr}\frac{\partial \Omega}{\partial X}. \tag{1}$$

Vorticity equation:

$$\Omega = -\nabla^2 \Psi. \tag{2}$$

Velocity equations:

$$U = \frac{\partial \Psi}{\partial Y}. \tag{3}$$

$$V = -\frac{\partial \Psi}{\partial X}. \tag{4}$$

Energy transport equation:

$$\frac{\partial \theta}{\partial t} + \vec{q} \cdot \vec{\nabla}\theta = \frac{1}{Pr}\nabla^2 \theta. \tag{5}$$

In addition, we require a set of boundary conditions for the flow. We model the attic space using a triangular cross-section and neglect building end effects. The boundaries of the attic are labelled as shown in Fig. 1.

We assume all boundaries to be solid, i.e. we consider a solid barrier which divides the attic lengthwise. Therefore, since there is no flow through any boundary, the stream function is constant along all boundaries. We hence define on all boundaries the streamfunction to be zero. Since the enclosure is bounded on all sides by fixed impermeable walls, we require that velocities are zero on all boundaries.

We define the non-dimensional temperature on boundary 1 to be zero, and that along boundary 2 to be one. We also define boundary 3 to be insulated, so there is no heat transfer through this boundary. (This is in accordance with the symmetry of the attic.) We hence require the condition given in Eq. (6):

$$\left.\frac{\partial \theta}{\partial X}\right|_{\text{boundary 3}} = 0. \tag{6}$$

Now whilst boundary 3 is solid, we wish to be able to compare our results with those of previous researchers

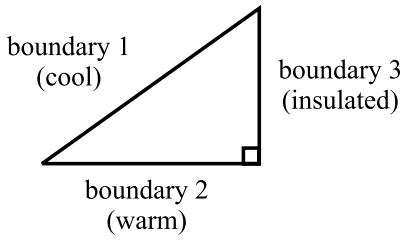

Fig. 1. Simple model plan.

Table 1
Boundary conditions along the boundaries shown in Fig. 1

Boundary	1	2	3
Velocity	$U = V = 0$	$U = V = 0$	$U = V = 0$
Temperature	$\theta = 0$	$\theta = 1$	$\frac{\partial\theta}{\partial X} = 0$
Stream function	$\psi = 0$	$\psi = 0$	$\psi = 0$
Vorticity	Compute	Compute	$\Omega = 0$

such as Hasani and Chung [4] and Salmun [7]. Both defined vorticity on boundary 3 to be zero, so initially we do the same. We do, however, need to calculate the vorticity along boundaries 1 and 2.

The boundary conditions are summarised in Table 1.

3. Method of solution

A 41×41 rectangular finite-difference grid is placed over the triangular enclosure so that the diagonal elements coincide with points on the inclined surface (boundary 1). Node $(0,0)$ corresponds to the junction between boundaries 1 and 2, node $(40,0)$ to the right-angled corner and node $(40,40)$ to the top corner of the attic, as shown in Fig. 2.

Following Hasani and Chung [4], we attempt to solve the equations as follows:

1. Solve for vorticity everywhere except on boundaries using the vorticity transport equation. The vorticity transport equation is separated using the Peaceman–Rachford alternating direction implicit (ADI) (Lapidus and Pinder [5]) technique into two Eqs. (7) and (8):

$$\left[\frac{\partial\Omega}{\partial t}\right]^{\left(t+\frac{1}{2},t\right)} + \left[U\frac{\partial\Omega}{\partial X}\right]^{t+\frac{1}{2}} + \left[V\frac{\partial\Omega}{\partial Y}\right]^{t} = \left[\frac{\partial^2\Omega}{\partial X^2}\right]^{t+\frac{1}{2}} + \left[\frac{\partial^2\Omega}{\partial Y^2}\right]^{t} + \frac{Ra}{Pr}\left[\frac{\partial\theta}{\partial X}\right]^{t}, \tag{7}$$

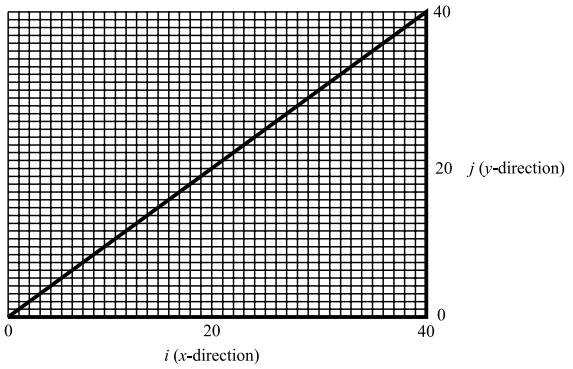

Fig. 2. Finite-difference grid for a triangular enclosure.

$$\left[\frac{\partial\Omega}{\partial t}\right]^{\left(t+1,t+\frac{1}{2}\right)} + \left[U\frac{\partial\Omega}{\partial X}\right]^{t+\frac{1}{2}} + \left[V\frac{\partial\Omega}{\partial Y}\right]^{t+1} = \left[\frac{\partial^2\Omega}{\partial X^2}\right]^{t+\frac{1}{2}} + \left[\frac{\partial^2\Omega}{\partial Y^2}\right]^{t+1} + \frac{Ra}{Pr}\left[\frac{\partial\theta}{\partial X}\right]^{t}. \tag{8}$$

An upwind scheme is applied to ensure the stability of the advective terms, and centred space schemes for the second derivatives and the $\partial\theta/\partial X$ term. It may be noted that values for velocities and temperature at time-step t are used, since we have not yet solved for these variables at time $(t+1)$. This will yield a tridiagonal system which may be solved using the Thomas algorithm.

2. Solve for stream function everywhere except on boundaries using the vorticity equation. We apply centred space schemes to the vorticity equation (2) and solve completely for the stream function at all points not on the boundaries. The stream function is solved completely at each time interval using the Gauss–Seidel iteration technique.

3. Solve for velocity everywhere except on boundaries using the velocity equations (3) and (4). This is simply performed by applying centred space schemes to the velocity equations and solving at each point in the attic.

4. Solve for vorticity on boundaries 1 and 2. Several finite-difference schemes were tried for vorticity on boundaries 1 and 2. However, all led to equations which were unstable upon application. It is suspected that Hasani and Chung [4] experienced similar difficulties, for they apparently did not directly apply finite-difference techniques either. Instead, they used Jenson's polynomial (Jenson [6]) as an approximation for stream function, and hence were able to obtain Eqs. (9) and (10) for boundary vorticities.

For boundary 1,

$$\Omega_{i,i} = \frac{-8\Psi_{i+1,i} + \Psi_{i+2,i}}{2\Delta X^2} + \frac{-8\Psi_{i,i-1} + \Psi_{i,i-2}}{2\Delta Y^2}, \quad 2 \leqslant i \leqslant 38. \tag{9}$$

For boundary 2,

$$\Omega_{i,0} = \frac{-8\Psi_{i,1} + \Psi_{i,2}}{2\Delta Y^2}, \quad 2 \leqslant i \leqslant 39. \tag{10}$$

5. Solve for temperature using the energy transport equation. The energy transport equation (5) is also separated using the Peaceman–Rachford ADI technique into two Eqs. (11) and (12):

$$\left[\frac{\partial\theta}{\partial t}\right]^{\left(t+\frac{1}{2},t\right)} + \left[U\frac{\partial\theta}{\partial X}\right]^{t+\frac{1}{2}} + \left[V\frac{\partial\theta}{\partial Y}\right]^{t} = \frac{1}{Pr}\left(\left[\frac{\partial^2\theta}{\partial X^2}\right]^{t+\frac{1}{2}} + \left[\frac{\partial^2\theta}{\partial Y^2}\right]^{t}\right), \tag{11}$$

$$\left[\frac{\partial\theta}{\partial t}\right]^{\left(t+1,t+\frac{1}{2}\right)}+\left[U\frac{\partial\theta}{\partial X}\right]^{t+\frac{1}{2}}+\left[V\frac{\partial\theta}{\partial Y}\right]^{t+1}=\frac{1}{Pr}\left(\left[\frac{\partial^2\theta}{\partial X^2}\right]^{t+\frac{1}{2}}+\left[\frac{\partial^2\theta}{\partial Y^2}\right]^{t+1}\right). \quad (12)$$

An upwind scheme is again applied to ensure the stability of the advective terms, and centred space schemes for the second derivatives. We use values for velocity at time $(t+1)$ since these are now available. This will yield a tridiagonal system which may be solved using the Thomas algorithm.

6. Temperature is well defined for boundaries 1 and 2, so we need only consider boundary 3. Since velocities are zero on the boundaries and we have the insulation property (6), the energy transport equation (5) reduces to Eq. (13):

$$\frac{\partial\theta}{\partial t}=\frac{1}{Pr}\left(\frac{\partial^2\theta}{\partial X^2}+\frac{\partial^2\theta}{\partial Y^2}\right). \quad (13)$$

If we imagine a set of fictitious points with $i=41$, i.e. $(41,j)$, $j=0,\ldots,40$, then by Eq. (6), we may define temperature at these nodes such that $\theta^t_{41,j}=\theta^t_{39,j}$. A centred space scheme may now be applied to the $\partial^2\theta/\partial X^2$ term.

This reduces (13) to a tridiagonal system which may be solved using the Thomas algorithm.

4. Results

4.1. Simple model

Flow within a triangular enclosure representing the attic with heated base, cooled inclined surface and insulated (adiabatic) vertical side has been modelled as previously described. Values of 710, 7100, 71 000 and 710 000 have been used for the Rayleigh number, whilst 0.71 has been used for the Prandtl number. Following Hasani and Chung [4], a 41×41 grid has been used and slopes for the inclined surface of 1.0, 0.5 and 0.2 analysed using $\Delta x=\Delta y$, $\Delta x=2\Delta y$ and $\Delta x=5\Delta y$ respectively.

The simple model considers the steady state solution for flow in the triangular attic. This solution has been obtained by developing a computer code to solve Eqs. (7)–(13) and running the code until convergence is achieved.

Figs. 3 and 4 show results for streamlines and temperature contours for the various flow conditions. Since we are dealing with steady flow, the streamlines are equivalent to the paths followed by individual particles in the fluid. These results resemble closely those obtained by both Hasani and Chung [4] and Salmun [7].

The magnitude of the non-dimensional stream function increases approximately linearly with an increase in Rayleigh number, as may be observed from the maximum value of the stream function in each case.

Using the velocity equations we can establish that streamlines with positive Ψ correspond to anticlockwise circulation, and those with negative Ψ correspond to clockwise circulation. This means that for singled-cell flow as occurs for low Rayleigh numbers (Fig. 3), flow is anticlockwise. The air mass moves along the base to the vertical wall where, have gained heat from the base, it rises up the wall. When it reaches the cold roof, its heat is lost and the air falls down along the inclined surface.

As the Rayleigh number is increased, there is a propensity for multicellular flow to develop. Whilst such Rayleigh–Bernard convection might be expected for a fluid heated from below, it was not observed in the numerical models of Poulikakos and Bejan [2], who also used a second order finite-difference scheme, and del Campo et al. [3], who used a Galerkin finite element scheme. Poulikakos and Bejan [2] did, however, discuss the possibility of such convection, drawing attention to the experimental study by Poulikakos and Bejan [8]. These observations were the basis on which Bejan [9] wrote, "...at high enough Rayleigh numbers and in shallow enough triangular spaces cooled from above, the flow will opt for the multicellular Bánard pattern characteristic of layers heated from below." The first numerical model of multicellular flow in a triangular-shaped space was that by Salmun [7], who used a second order leapfrog scheme, and this result was supported by Hasani and Chung [4], who used the third order accurate QUICK scheme. Compared with the very even temperature gradient for single-celled flow, the temperature distributions for multicellular flow suggest that the fluid is well mixed. As the number of cells increases, we therefore expect the temperature to be more uniform throughout the enclosure.

The shift to multicellular flow is encouraged by a decrease in slope of the inclined surface. An excellent illustration of this is the case $Ra=710\,000$ (Fig. 4), wherein a slope of 1.0 gives three cells, whilst slopes of 0.5 and 0.2 give 5- and 7-cell flows respectively. It is postulated that multicellular flow develops due to viscous effects which do not allow particles to push past one another freely. As the slope is decreased, there is increased friction between particles moving to the left down the inclined surface and those moving to the right along the base. The single-celled flow cannot be maintained under these conditions. Multicelled flow results, in which neighbouring cells circulate in opposite directions so that, near the border between the two cells, the flows are in the same direction.

Whilst the critical Rayleigh number at which the flow becomes multicellular, Ra_c, has not been determined exactly, the results do indicate that for slope 0.2, Ra_c lies in the range 710–7100. This is in agreement with both the numerical model by Salmun [7], which predicted

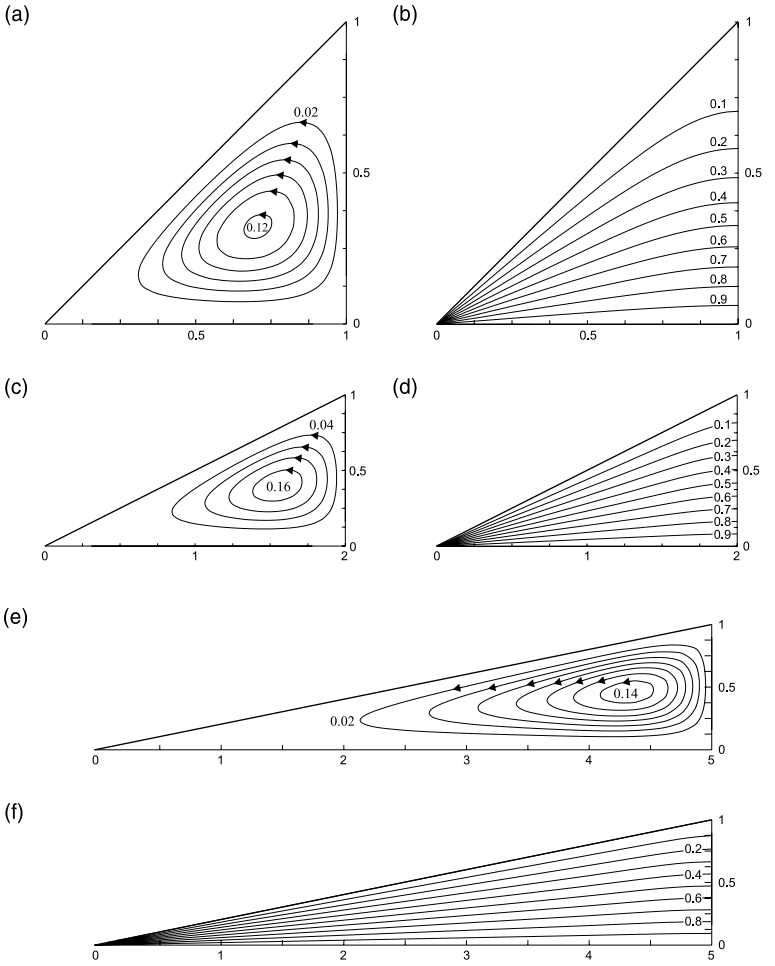

Fig. 3. (a,c,e) Streamlines and (b,d,f) temperature contours for $Ra = 710$ and inclined surface slope 1.0, 0.5 and 0.2 respectively.

$Ra_c \approx 4500$, and the analytical value of ≈3000 obtained in a separate study by Salmun [10] using linear theory.

The strong correlation between these results and two other published sets validates the code for convection without inflow or outflow. We now consider application of this model to a real attic.

4.2. Real attic model

Most other investigations regarding natural convection in triangular-shaped regions have been aimed at modelling air flow in real attics. However, all have a fundamental problem: the magnitude of the Rayleigh number. In the study by Akinsete and Coleman [1], for example, the maximum value for Ra used was 4.5×10^4, whilst Hasani and Chung [4] stated that values of Ra as high as 10^6 were applicable in real enclosures. Values of this magnitude were also used in the other studies mentioned here.

The Rayleigh number is defined as

$$Ra = \frac{g\beta(T_h - T_{ref})H^3}{v\alpha}. \tag{14}$$

For a realistic attic of height 4 m, i.e. that of a large building, we obtain a value for Ra of 9.06×10^{10}, i.e. $Gr = Ra/Pr = 1.28 \times 10^{11}$. Hence for a realistic attic, $Ra = O(10^{11})$, and even for small buildings, we have $Ra > 10^{10}$.

Unfortunately, for such a large Ra, it is extremely difficult to obtain a stable model. This is perhaps not surprising, since in the vorticity transport equation (1) we have an extremely large coefficient on the right-hand side. In order to counter this, either the value for non-dimensional vorticity must be extremely large or there needs to be almost no variation of temperature in the x-direction.

From the simple model, we note that there is increased multicellular behaviour for increased Ra. This

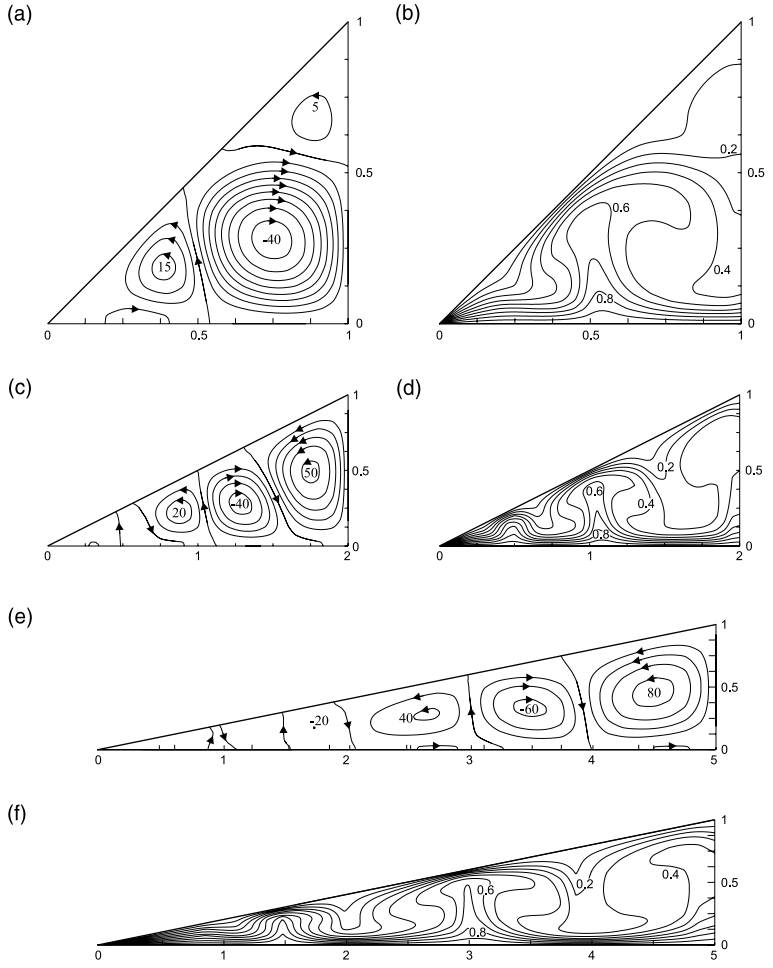

Fig. 4. (a,c,e) Streamlines and (b,d,f) temperature contours for $Ra = 710000$ and inclined surface slope 1.0, 0.5 and 0.2 respectively.

suggests that for realistic *Ra* the air must be extremely well mixed to the point where a 41×41 grid would be insufficient to model the multicellular structure of the flow. Indeed, it calls into question whether describing the flow as "multicellular" would be accurate for such a case, or whether the flow would be turbulent.

In order to improve stability at high Rayleigh and Grashof numbers, we consider the way in which we model boundary vorticity. Briley [11] used higher-order schemes for modelling boundary vorticity which are claimed to be stable for high *Ra* flows. However, in a triangular-shaped space it is extremely difficult to implement such schemes near the corners. In particular, Briley's scheme requires four points within the solution domain (in our case, the attic), and in the corners we would have to have an excessive number of nodes outside the actual flow in order to implement the scheme. Simply refining the grid would not solve this problem, since it is a problem associated with the scheme, not the grid resolution. We would therefore need to use a lower order scheme near the corners of the flow, and using different schemes to calculate boundary vorticity at different locations is likely to lead to instabilities. Indeed, no stable model was obtained for such a case.

Therefore, in order to obtain a stable model at high Rayleigh and Grashof numbers, we define vorticity on the boundaries to be zero.

Consider a realistic Rayleigh number of 7.1×10^{10}, i.e. $Gr = 10^{11}$. Fig. 5 shows streamlines and temperature contours for an inclined surface of slope 0.5.

Initial inspection of the streamlines in Fig. 5(a) suggests that we have taken a big step backwards, since now the flow is dominated by a single cell, and we stated previously that a high Rayleigh or Grashof number should result in many cells. However, we also suggested that multicellular flow should result in thorough mixing of the air, and hence an almost uniform temperature distribution. The temperature distribution in Fig. 5(b) strongly supports this.

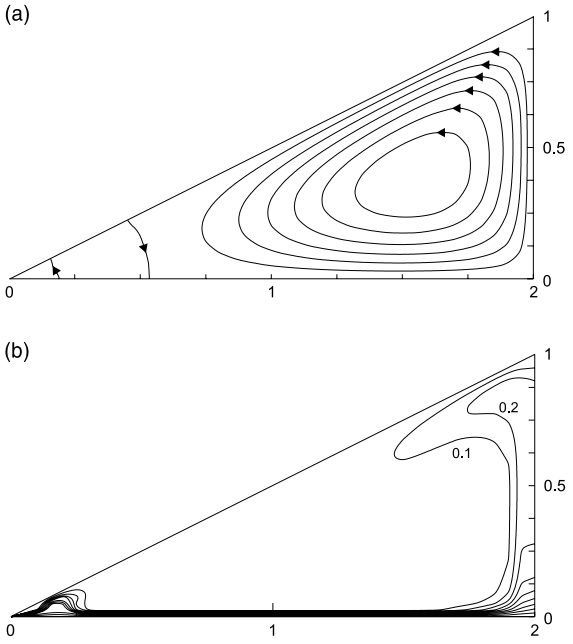

Fig. 5. (a) Streamlines and (b) temperature contours for $Gr = 10^{11}$.

In order to verify this result, we consider the temperature distribution for various values of the Grashof number. The "uniform" temperature distribution evolves slowly as the Grashof number is increased as expected. The surprising result is that whilst the temperature within the attic is almost uniform, it is uniformly cold!! The temperature throughout the attic is close to that of the cold surface, and the warm surface below provides very little heating at all! We would expect this effect to be accentuated by any insulation present between the attic space and rooms below.

Perhaps even more surprising is that this temperature distribution results solely from the gravity term in the conservation of momentum equations. In other words, the temperature distribution in the attic is almost solely governed by gravity.

4.3. Real attic model incorporating inflows and outflows

We now modify the model to allow air to flow into and out of the system through the vertical and horizontal boundaries. This models air of a given temperature being pumped into and circulated through the attic.

We must ensure that mass is conserved in the system, so the amount of air we pump into the system must be the same as that which exits. We also attempt to account for the walls around the enclosure, since the thermal conductivity of the boundaries will affect the temperature distribution of the attic for given external (outside) temperature and given temperature of the rooms below. We therefore define further boundary conditions and modify the energy Eq. (15), since thermal conductivity is no longer constant over all space:

$$\rho c_p \frac{DT}{Dt^*} = \lambda \nabla^2 T. \tag{15}$$

Our aim is to observe the effects of an inflow/outflow system on the temperature distribution of the attic. Such results could be of benefit for a variety of temperature-related problems in buildings. Further, we may suspect that for sufficiently high inflow velocity, the instabilities observed previously should be reduced, so there is a chance that we may obtain results which are applicable to a real attic of appropriate Grashof number.

For fluids in which thermal conductivity is not constant, the energy Eq. (15) should read

$$\rho c_p \frac{DT}{Dt^*} = \vec{\nabla} \cdot (\lambda \vec{\nabla} T). \tag{16}$$

It may be noted that this is normally the case for compressible fluids since thermal conductivity varies with density.

After non-dimensionalisation, Eq. (16) may be rewritten to give a new energy transport equation:

$$\frac{\partial \theta}{\partial t} + \vec{q} \cdot \vec{\nabla} \theta = \frac{1}{\mu c_p} \vec{\nabla} \cdot (\lambda \vec{\nabla} \theta). \tag{17}$$

We allow air to flow in and out at specific points on the boundaries. Consequently, the stream function must take a constant value on each section of boundary which does not have an inflow or outflow.

Consider a system with an inflow on the horizontal base and an outflow on the vertical wall. We suppose that the streamline passing from the centre of the inflow to the centre of the outflow corresponds to $\Psi = 0$. We therefore expect that the stream function at the node to one side of the inflow will be the negative of that to the other side. Using the velocity equation (4), we may define values for stream function on either side of the inflow as follows:

$$\Psi_{i+1,0} = -v_{\text{in}} \Delta X, \tag{18}$$

$$\Psi_{i-1,0} = v_{\text{in}} \Delta X. \tag{19}$$

For a system with an inflow on the horizontal boundary and an outflow on the vertical surface, we should therefore have the boundary stream function distribution shown in Fig. 6. The stream function may be derived in a similar manner for other inflow and outflow locations and for multiple inflow/outflow systems.

Since the boundary nodes in this model represent the solid walls surrounding the fluid rather than the fluid itself, we are now able to define vorticity as zero on all boundaries without loss of generality.

We require velocities on the boundaries to be zero except at the inflow and outflow points. We have already defined temperature on boundaries 1 and 2, and we solve for temperature on boundary 3 as before. The

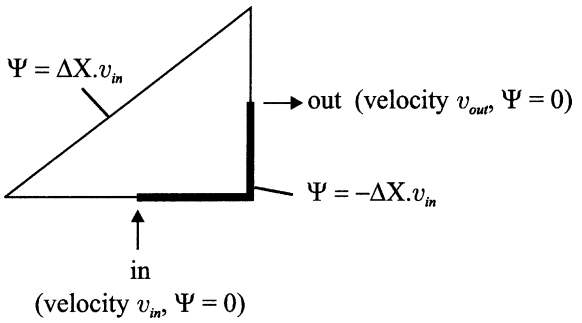

Fig. 6. Stream function for an inflow on the horizontal boundary and outflow on the vertical boundary.

temperature of air entering the attic through the inflow is defined to be θ_{in}.

We solve for temperature using the Peaceman–Rachford technique combined with an upwind scheme as before. However, we now need to incorporate variable thermal conductivity. The ADI technique now separates Eq. (17) into Eqs. (20) and (21):

$$\left[\frac{\partial\theta}{\partial t}\right]^{\left(t+\frac{1}{2},t\right)} + \left[U\frac{\partial\theta}{\partial X}\right]^{t+\frac{1}{2}} + \left[V\frac{\partial\theta}{\partial Y}\right]^{t} = \frac{1}{\mu c_p}\left(\frac{\partial}{\partial X}\left[\lambda\frac{\partial\theta}{\partial X}\right]^{t+\frac{1}{2}} + \frac{\partial}{\partial Y}\left[\lambda\frac{\partial\theta}{\partial Y}\right]^{t}\right), \tag{20}$$

$$\left[\frac{\partial\theta}{\partial t}\right]^{\left(t+1,t+\frac{1}{2}\right)} + \left[U\frac{\partial\theta}{\partial X}\right]^{t+\frac{1}{2}} + \left[V\frac{\partial\theta}{\partial Y}\right]^{t+1} = \frac{1}{\mu c_p}\left(\frac{\partial}{\partial X}\left[\lambda\frac{\partial\theta}{\partial X}\right]^{t+\frac{1}{2}} + \frac{\partial}{\partial Y}\left[\lambda\frac{\partial\theta}{\partial Y}\right]^{t+1}\right). \tag{21}$$

4.3.1. Single inflow system

Consider placing an inflow with temperature $\theta_{\text{in}} = 1$ and velocity v_{in} along the horizontal base. The air is allowed to flow out at a point on the vertical wall. This situation is considered for $Gr = 10^{11}$.

Fig. 7 gives streamlines and temperature contours for inflow velocity 2×10^5 (corresponding to 0.714 ms^{-1}). Since we are interested in increasing the temperature on the inclined surface, we place the inflow close to the inclined surface. We locate the outflow halfway up the vertical wall; for an inclined surface of slope 0.5, the outflow corresponds to $(X, Y) = (2, 1/2)$. As expected, the inflow increases the temperature along the bottom of the attic and induces air flow directly from the inflow point to the outflow point. As the inflow/outflow velocities are increased, this effect is more pronounced, but qualitatively very similar.

If we wish to place the inflow on the vertical surface, we must clearly place it above the outflow, since otherwise it would be pushing against the natural flow, and the inflowing air would be pushed straight up to the outflow.

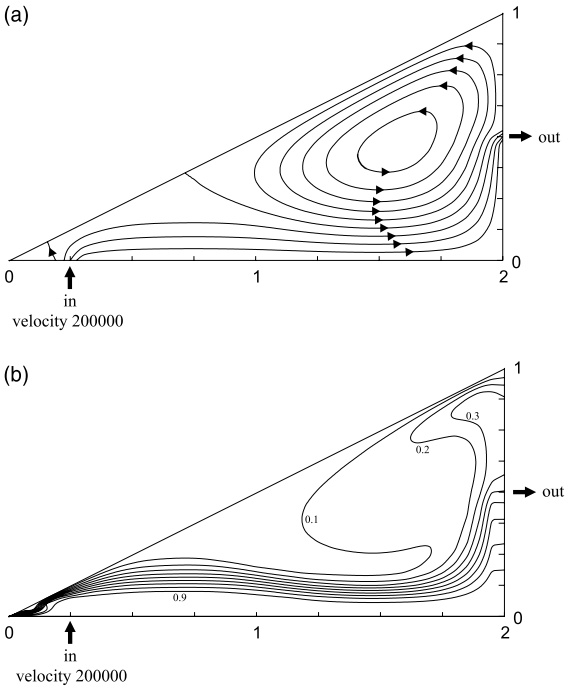

Fig. 7. (a) Streamlines and (b) temperature contours for $Gr = 10^{11}$, slope 0.5 with inflow at $(1/4, 0)$, velocity 200 000, and outflow at $(2, 1/2)$.

Placing the inflow higher on the wall should result in the inflow being enhanced by the natural flow. This has been tested by considering inflow position $(2, 7/8)$, for which results are given in Fig. 8. The inflow velocity is again 2×10^5 and the inflow temperature is 1.0.

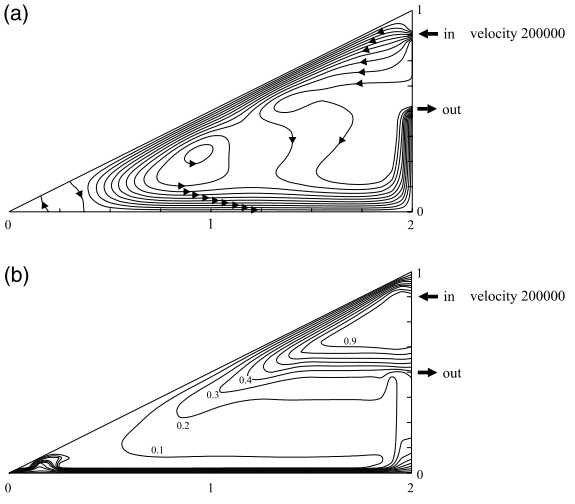

Fig. 8. (a) Streamlines and (b) temperature contours for $Gr = 10^{11}$, slope 0.5 and inflow velocity 2×10^5 for inflow on the vertical boundary and outflow halfway up the vertical boundary.

4.3.2. Multiple inflow system

Consider now placing two inflows on the horizontal boundary in order to increase the air temperature of the attic. Consider inflows at positions $(1/4, 0)$ and $(3/4, 0)$ with an inflow velocity of 2×10^5 at each location. The outflow remains at $(2, 1/2)$. We define the stream function on the boundaries in order to account for the various inflows and outflow. This is done as previously described, and boundary stream functions can be defined as shown in Fig. 9. Results for this case are shown in Fig. 10.

A comparison between Figs. 7(a) and 10(a) indicates that when the second inflow is present, the natural circulation is less influential on the overall circulation within the attic, i.e. the region which is continually circulating in the attic is smaller. This is not surprising since we are now pumping twice the volume of air through the attic in the same amount of time. A comparison between Figs. 7(b) and 10(b) suggests that the extra inflow has little effect on the temperature in the bottom left-hand corner, but has a significant effect on the temperature in the top corner. The second inflow at $(3/4, 0)$ would thus be advantageous if we are concerned with heating the whole inclined surface.

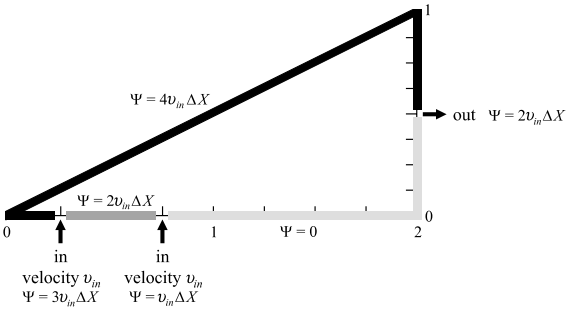

Fig. 9. Summary of defined stream function values on boundaries for two inflows at $(1/4, 0)$ and $(3/4, 0)$, each with inflow velocity v_{in}, and outflow at $(2, 1/2)$.

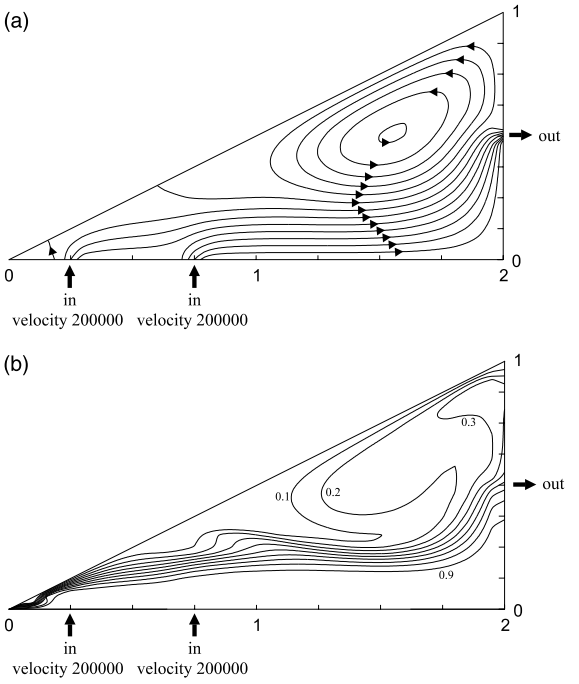

Fig. 10. (a) Streamlines and (b) temperature contours for $Gr = 10^{11}$, slope 0.5, with inflows at $(1/4, 0)$ and, $(1/2, 0)$ and outflow at $(2, 1/2)$.

5. The Copper Chase attic

The Copper Chase attic is divided into three sections, two symmetric triangular prisms separated by a narrow corridor. The width of the building is about 24 m, so the length of each triangular cross-section is about 11 m. The roof has slope $512 \approx 0.417$, so the height of the triangular cross-section is about 4.58 m. We attempt to model air flow in one of the triangular sections. For this slope, X varies from 0 to $12/5$, whilst Y varies from 0 to 1. The Grashof number for the Copper Chase attic is $Gr \approx 2 \times 10^{11}$.

The roof material (i.e. the inclined surface) is plywood with metal on the outside. Metals have a far greater thermal conductivity than plywood, so we may neglect any temperature gradient across the metal as being negligible compared with that across the plywood. The vertical walls of the corridor are made of plywood, and we assume the ceiling is insulated with glass wool (fibreglass).

We assume that the boundary nodes of our finite-difference grid have thermal conductivities corresponding to these materials and that the rest of the grid has the thermal conductivity of air. For a 41×41 grid, the distance between each node in the y-direction will be about 11.5 cm, which is not unreasonable for the insulation layer. For situations in which we have an inflow or outflow, the conductivity of the appropriate boundary nodes is set to the value for air.

Firstly, we consider the actual temperature distribution in the Copper Chase attic, i.e. we model the attic with no inflow or outflow as is the case for the real attic. We assume the air temperature along the horizontal base is 10 °C. The resulting streamlines and temperature contours are shown in Fig. 11. The attic is of almost uniform temperature, i.e. very close to the temperature of the inclined surface.

A single inflow is added at $(x, y) = (11/8, 0)$, i.e. node $(5, 0)$, and an outflow at $(x, y) = (11, 2.29)$, i.e. node $(40, 20)$. The model is run for inflow velocities of 0.5 and 1 ms^{-1}. Streamlines and temperature contours for these situations are shown in Fig. 12. As expected, the main cell is pushed towards the top corner of the attic, and we

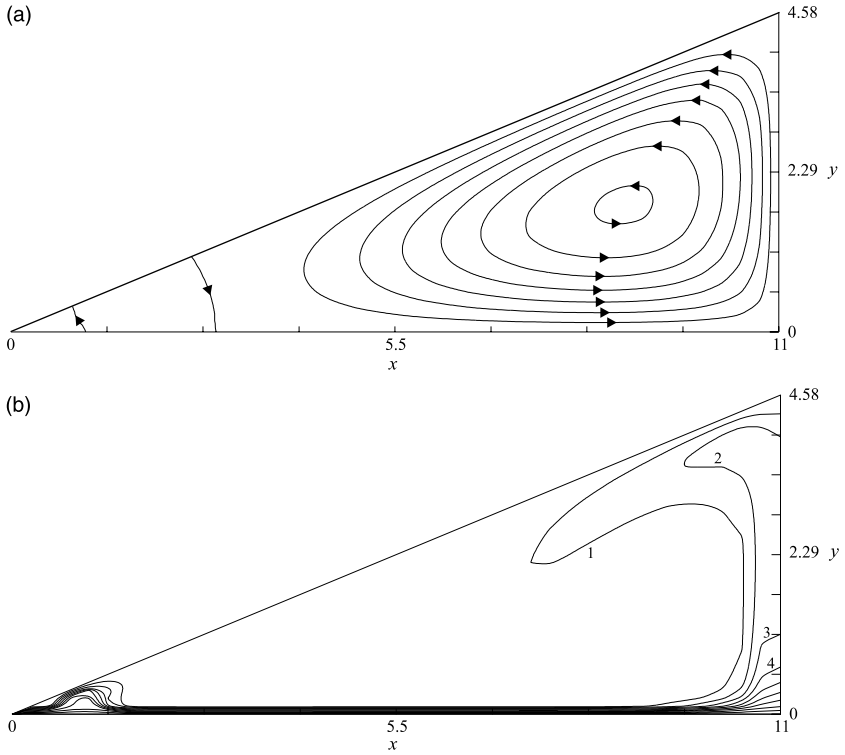

Fig. 11. (a) Streamlines and (b) temperature contours (°C) for the Copper Chase attic with no inflow/outflow.

see a significant increase in temperature within the attic space. These effects are enhanced by an increased inflow velocity, as the inflow becomes more dominant over the natural convection.

We now add a second inflow at $(33/8, 0)$, i.e. node $(15, 0)$. Results for this multiple-inflow situation are given in Fig. 13 for both inflow velocities. Clearly there is a dramatic increase in the attic air temperature, which again is enhanced by an increase in inflow velocity. The lower half of the attic is now well heated, including the region close to the inclined surface. This would hopefully lead to melting of the ice outside.

6. Results and conclusions

6.1. Flow in a triangular-shaped space

The simple model presented is able to model natural convection in a triangular-shaped space for low Rayleigh and Grashof numbers. The results obtained using this model are consistent with those obtained by previous researchers. For extremely low Grashof numbers, the flow is single celled. Multicellular flow patterns form if the Grashof number is increased or if the slope of the inclined surface is decreased. In such situations, there is increased mixing of the air, resulting in a tendency towards a uniform temperature distribution. Unfortunately, however, and contrary to the claims of previous researchers, the results obtained are not applicable to flow in a real attic, since for such a space the Grashof number is much greater.

In order to obtain a solution which is stable for realistic Grashof numbers, boundary vorticity has been defined to be zero. This produces results which show that, whilst an attic does indeed have an approximately uniform temperature distribution for realistic Grashof numbers, the temperature is little more than that of the cold inclined surface.

By allowing warm air to flow in through the horizontal base and out through the vertical wall, we are able to increase the temperature in the attic. This effect is enhanced by placing the inflow close to where the base meets the inclined surface, using a higher inflow velocity, and using more than one inflow into the system.

6.2. The Copper Chase attic

At the present time, the air in the Copper Chase attic is extremely cold. The temperature distribution is almost uniform and is approximately that of the inclined surface, which is why the ice is not melting. The addition of vents which allow air to pass from the warm third storey rooms into the attic should result in some increase in the

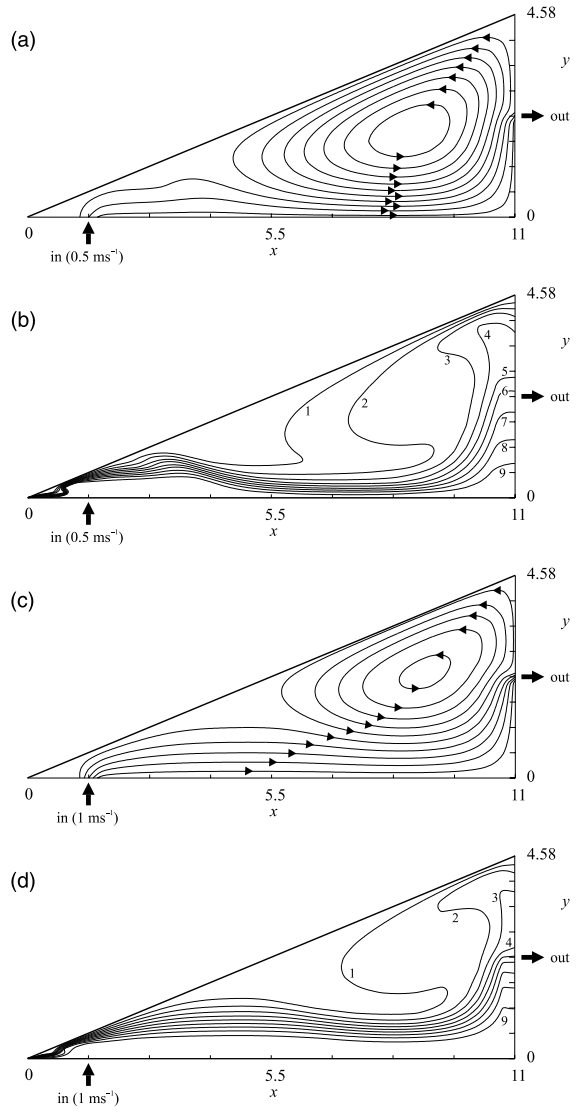

Fig. 12. (a,c) Streamlines and (b,d) temperature contours for the Copper Chase attic with inflow at $(11/8, 0)$ and outflow at $(11, 2.29)$, and inflow velocity 0.5 and 1 ms^{-1} respectively.

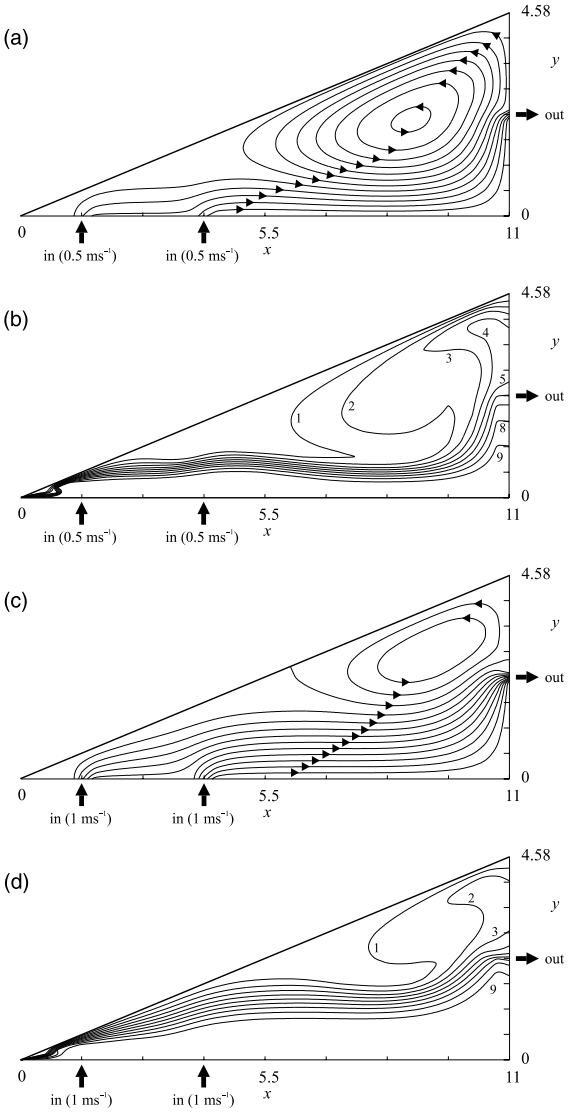

Fig. 13. (a,c) Streamlines and (b,d) temperature contours (°C) for the Copper Chase attic with inflows at $(11/8, 0)$ and $(33/8, 0)$ and outflow at $(11, 2.29)$. (a,b) Correspond to inflow velocity 0.5 ms^{-1}, whilst (c,d) correspond to inflow velocity 1 ms^{-1}.

attic temperature. Using fans to pump air into the attic at higher velocities would enhance this effect, as would the use of multiple vents. Hence there is the potential for melting to occur, which would eliminate the problem of ice collection on the roof, and at the same time remove some of the excess heat from the third floor.

6.3. Conclusions

This study has demonstrated the ability of the model to reproduce the results of previous investigations, develop solutions for realistic Grashof numbers, and examine the effect of installing active vents in the ceilings of the top floor units at Copper Chase. The results from these simulations are consistent with qualitative information that the attic is indeed very cold during the winter months.

Additional data not currently available needs to be collected to verify the model thoroughly. Once this is available, further processes can be included in the model, e.g. better definition of the roofing and insulation material thermal properties, examining building end effects through a three-dimensional model, including a turbulence model to accommodate such a high Grashof

number. However, without any definitive data to justify further extensions, the current model has provided an initial solution to the two problems, i.e. install ceiling fans.

References

[1] V.A. Akinsete, T.A. Coleman, Heat transfer by steady laminar free convection in triangular enclosures, Int. J. Heat Mass Transfer 25 (7) (1982) 991–998.
[2] D. Poulikakos, A. Bejan, The fluid dynamics of an attic space, J. Fluid Mech. 131 (1983) 251–269.
[3] E.M. del Campo, M. Sen, E. Ramos, Analysis of laminar natural convection in a triangular enclosure, Numer. Heat Transfer 13 (1988) 353–372.
[4] S.M.F. Hasani, B.T.F. Chung, Laminar natural convection in a triangular enclosure, Proc. ASME Ocean Eng. Div. 14 (1997) 107–116.
[5] L. Lapidus, G.F. Pinder, Numerical Solution of Partial Differential Equations in Science and Engineering, Wiley, New York, 1982.
[6] V.G. Jenson, Viscous flow around a sphere at low Reynolds numbers ($\leqslant 40$), Proc. R. Soc. London, Ser. A 249 (1959) 346–366.
[7] H. Salmun, Convection patterns in a triangular domain, Int. J. Heat Mass Transfer 38 (2) (1995) 351–362.
[8] D. Poulikakos, A. Bejan, Natural convection experiments in a triangular enclosure, J. Heat Transfer 105 (1983) 652–655.
[9] A. Bejan, in: Convection Heat Transfer, Wiley, New York, 1984, p. 196.
[10] H. Salmun, The stability of a single-cell steady state solution in a triangular enclosure, Int. J. Heat Mass Transfer 38 (2) (1995b) 363–369.
[11] W.R. Briley, A numerical study of laminar separation bubbles using the Navier-Stokes equations, J. Fluid Mech. 47 (1971) 713–736.